Design of a multi-object, high throughput, low resolution fiber spectrograph for WFMOS

Stephen A. Smee*[a], Robert H. Barkhouser[a], Karl Glazebrook[b]
[a]Instrument Development Group, Johns Hopkins University, Baltimore, MD USA 21218
[b]Department of Physics and Astronomy, Johns Hopkins University, Baltimore, MD USA 21218

ABSTRACT

We present the preliminary optical and optomechanical design of a high throughput, fiber spectrograph for the Gemini/Subaru Wide-Field, Fiber-Fed, Multi-Object Spectrograph (WFMOS) designed with the principle goal of studying the nature of dark energy via enormous high-redshift spectroscopic surveys. Developed from an original Sloan Digital Sky Survey design this multi-object spectrograph utilizes all-refractive cameras, volume phase holographic gratings, and state-of-the-art CCD detectors to produce a peak instrument throughput of ~ 70%. The instrument produces 292 spectra simultaneously in two channels covering the bandpass $390 < \lambda < 1000$ nm with a mean spectral resolution, λ/FWHM, of R ~ 1700. WFMOS will employ approximately ten of these fiber spectrographs on an 8 m class telescope to capture nearly 3000 spectra simultaneously. When used in a nod & shuffle mode of operation these spectrographs will facilitate spectroscopy of faint $0.5 < z < 3.5$ galaxies with unprecedented efficiency.

Keywords: WFMOS, Gemini telescope, Subaru telescope, multi-object spectrograph, fiber spectrograph, spectrograph, VPH grating, optical design, optomechanical design, camera

1. INTRODUCTION

The Gemini Observatory and the National Astronomical Observatory of Japan (NAOJ) have committed to investigating the development of a next-generation wide-field spectroscopic survey instrument referred to as the Wide-Field, Fiber-Fed, Multi-Object Spectrograph (WFMOS). The impetus for this investigation is the desire to answer several key questions facing today's astronomy community. What is dark energy? How does its equation of state vary as a function of time? What is the nature of dark matter on galactic scales? What formation mechanisms result in the observed structure of our Galaxy? Why is our Galaxy different in structure from other local group members? How does galaxy formation and evolution depend on the formation and evolution of large scale structure? How was the Universe reionized? What mechanisms govern the creation and dispersal of metals in the Universe?

WFMOS will provide the ability to collect detailed spectroscopy from millions of objects over thousands of square degrees of sky, thus overcoming the statistical complexity of the Universe and allowing us to investigate these fundamental questions. A primary design goal is the spectroscopic resolutions of 'baryon oscillations' over cubic Gigaparsecs of space in order to study the nature of dark energy via its effect on standard measuring rods.[1] Mounted at the prime focus of either the Gemini or Subaru telescopes, the instrument will be capable of producing simultaneous moderate to high resolution (R = 1,000 - 40,000) spectra from approximately 4500 targets, in a 1.5 degree field, over a spectral window $390 < \lambda < 1000$ nm. At a rate of ~ 20,000 spectra per night, WFMOS will be a unique instrument yielding a factor of 10-100 advantage over existing and planned multi-object spectrographs.

To collect such a large number of simultaneous spectra over a wide resolution range requires that WFMOS be comprised of multiple instrument subsystems: a wide-field multi-element corrector, an atmospheric dispersion corrector (ADC), an Echidna-style fiber positioner, approximately ten low resolution spectrographs, and multiple high resolution spectrographs. Not to mention copious amounts of control and data reduction software. The corrector, ADC, and fiber postitioner will be mounted at prime focus. The spectrographs will be stationary and located below the telescope floor. A large fiber bundle transmits the light from the positioner to the spectrographs.

* smee@pha.jhu.edu; phone 1 410 516-7097; fax 1 410 516-6664; idg.pha.jhu.edu

Ground-based and Airborne Instrumentation for Astronomy, edited by Ian S. McLean, Masanori Iye,
Proc. of SPIE Vol. 6269, 62692I, (2006) · 0277-786X/06/$15 · doi: 10.1117/12.672186

In this paper a preliminary optical and optomechanical design for the WFMOS low resolution spectrographs is presented. The design is based on the Sloan Digital Sky Survey (SDSS) spectrographs, which were a near perfect match to the WFMOS requirements; the heritage and excellent performance of the SDSS spectrographs are also motivating factors. Section 2 provides a summary of the requirements and considerations that influenced the design. In addition, a brief description of the SDSS spectrograph parameters is provided as a point of comparison. Section 3 presents the optical design and discusses its performance, i.e. image quality, resolution, and throughput. Section 4 describes the optomechanical design of the instrument.

2. REQUIREMENTS, GOALS, AND GENERAL CONSIDERATIONS

2.1. Wavelength coverage

The required spectral window for WFMOS is $390 < \lambda < 1000$ nm. This range is a compromise arbitrated by several factors: the dark energy science requirement to measure redshifts in the range $0.5 < z < 3.5$, the atmospheric cutoff at 350 nm, and the silicon (CCD) cutoff at 1000 nm.

2.2. Resolution

The three main science cases for WFMOS, dark energy, galaxy genesis, and stellar archaeology, each impose requirements on resolution. For the dark energy science, redshifts need only be accurate to ~ 600 km/s and a resolution of R ~ 500 would suffice for this requirement. For the galaxy genesis science the goal is to provide a kinematic accuracy of < 20 km/s in order to assign a star to a given stellar population. This requires a resolution of R ~ 2000. The stellar archaeology science requires comparable resolution.

Hence, to satisfy all three science cases one would like to have a resolution of R ~ 2000. It is worth noting that there is some benefit in going higher in the red. The benefit being that the red end of the spectrum is thick with OH lines and at R ~ 3000 one can cleanly resolve the [OII] doublet assuring a secure line identification.

2.3. Throughput

The goal for throughput is to maintain or exceed the predictions laid out in the K.A.O.S. Purple Book.[2] K.A.O.S. (Kilo-Aperture Optical Spectrograph) is the concept for a highly multiplexed wide-field, prime focus, multi-object spectrograph for the Gemini Observatory, which served as the baseline design for the WFMOS feasibility study. Briefly, the K.A.O.S. predictions were ~ 37% peak instrumental efficiency and ~ 23% peak system efficiency, assuming single channel R = 1000 spectrographs.

2.4. Nod & Shuffle Observing

Faint object sky subtraction will be done using nod & shuffle observing. This technique allows Poisson-limited sky subtraction for faint objects via rapid CCD charge-shuffling in synchrony with telescope nodding.[3] Nod & shuffle is particularly important for fiber spectroscopy as the galaxy targets for dark energy reach down to 1% of the night sky in brightness. Conventional fiber sky subtraction techniques are systematics-limited at this faintness.[4] A consequence is that the layout of spectra on the CCD must allow gaps for shuffled sky images.

2.5. Fibers

Light is coupled to the spectrographs through 200 μm diameter fibers at a focal ratio of 4. This size and focal ratio were chosen to minimize focal ratio degredation (FRD) and to match the 1 arcsecond, 100 μm diameter, fibers at the Echidna positioner.[5] A lenslet at the interface between the positioner and spectrograph fibers converts the f/2 primary beam to the FRD-optimized f/4 input.

The focal plane will consist of ~ 3000 “low resolution” fibers and ~ 1500 “high resolution” fibers. The number and distribution were set by the need to provide sufficient sampling of galaxies and stars over the 1.5 degree field of the instrument.

2.6. The Gemini and Subaru Telescopes

The K.A.O.S. Purple Book considered only a Gemini implementation of WFMOS. With the addition of the NAOJ as a partner the Subaru telescope became a potential platform as well. The Feasibility Study for WFMOS, upon which this work was based, investigated both telescopes as potential candidates, and throughput results are presented for both options.

At this writing (April 2006), the Subaru telescope is the baseline for WFMOS. This decision was made based on technical and cost considerations, many of which weighed in favor of the Subaru implementation.

2.7. The SDSS spectrographs

The requirements for the WFMOS low resolution spectrographs match very closely to the SDSS spectrograph parameters. SDSS[6] employs two fiber-fed, multi-object, spectrographs mounted on a Cassegrain rotator behind the primary of the SDSS 2.5 m telescope. The instrument employs a dual-channel design with a common reflecting collimator and a dichroic to split the beam into two channels: a *blue* channel $390 < \lambda < 600$ nm, and a *red* channel $600 < \lambda < 920$ nm. In each channel, just downstream of the dichroic, a transmitting grism (a replicated grating on the hypotenuse of a BK7 prism) disperses the light, which is imaged by an all-refractive camera onto a SITe $2k^2$ CCD with 24 μm pixels. Each spectrograph accepts 320 fibers, 180 μm in diameter, from the telescope focal plane; light is incident on the fibers at f/5 and enters the spectrographs at f/4 due to FRD. Each fiber subtends 1 arcsecond on the sky. The resolution is R ~ 1800 and the peak throughput is an impressive 45%.

As built, the SDSS spectrographs are a very close match to the requirements for WFMOS.

3. OPTICAL DESIGN

3.1. Overview

The optical design of the WFMOS low resolution spectrograph is nearly identical to the SDSS design. It is a dual-channel design that provides one-shot wavelength coverage at R ~ 1700 from the blue end of the visible spectrum to the near IR. The design is optimized for high throughput, using a single-surface reflecting collimator and all-refractive cameras containing only ten AR-coated air/glass surfaces and no beam obscuration. For WFMOS the bandpass is

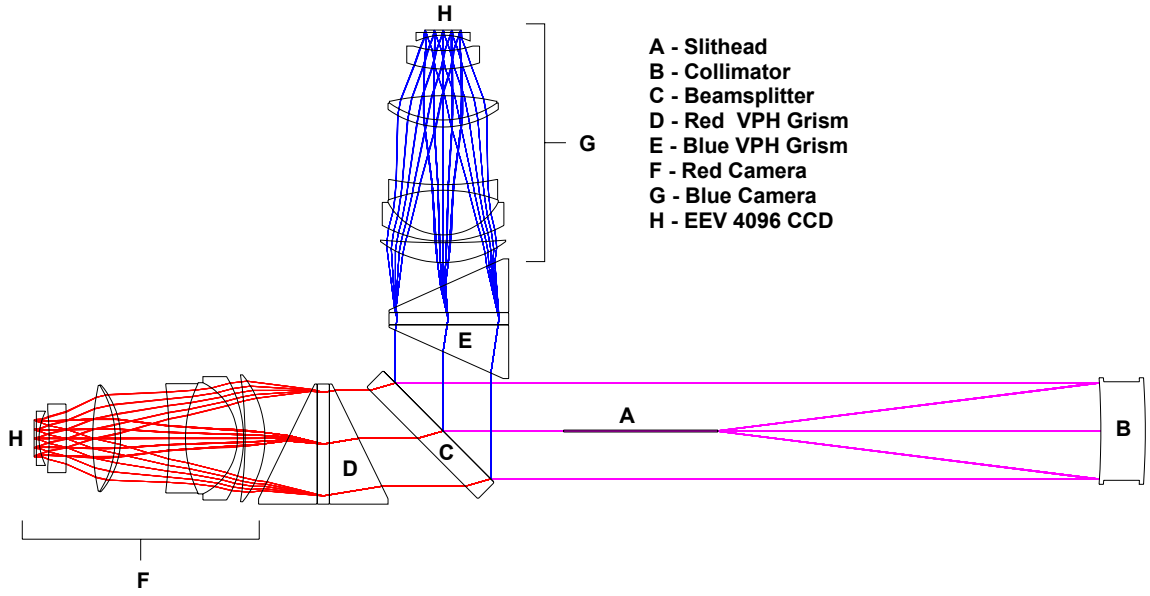

Figure 1. Optical layout of the WFMOS low resolution spectrograph design.

slightly broader than for SDSS, covering $390 < \lambda < 1000$ nm (SDSS coverage: $390 < \lambda < 920$ nm). Additionally, and most importantly, throughput is increased with the use of volume phase holographic (VPH) gratings and newer CCDs, resulting in an impressive 70% peak instrumental efficiency; a significant improvement over the 45% peak of the SDSS design.

Figure 1 shows the optical layout of the WFMOS low resolution spectrographs. Light enters the spectrograph through 200 μm fibers, which terminate at a curved slithead. The slithead positions the fibers on a radius concentric with the spherical collimating mirror, which transforms the f/4 output from the fibers to a 159 mm diameter collimated beam. The 45 degree dichroic beamsplitter reflects the blue portion of the bandpass ($\lambda < 640$ nm) and transmits the red wavelengths ($\lambda > 640$ nm). Immediately after the beamsplitter in each channel is a grism, containing a VPH grating sandwiched between two right prisms. The dispersed light exits the grisms and enters all-refractive, eight-element, f/1.5 cameras. Each camera contains a single $4k^2$ CCD with 15 μm pixels, which records the 292 first-order, full-bandpass spectra simultaneously. The camera demagnification from f/4 to f/1.5 produces fiber images that are 5 pixels in diameter, resulting in 5 pixel tall spectra on the detector. A fiber separation of 560 μm at the slithead produces a 14 pixel spectra-to-spectra spacing at the detector, leaving sufficient detector real estate between spectra to implement nod & shuffle observing. Additional detail on the spectrograph optics is given in the following sections.

3.1.1. Slithead

Light enters the spectrograph through fibers terminating at the slithead. For the preliminary design, we have assumed 200 μm diameter fibers with an f/4 output cone. The fibers are stacked vertically to form a long slit and are placed on a radius whose center of curvature coincides with that of the collimator. Additionally, the fibers are aimed in a fanlike pattern outward from the center of curvature toward the collimator, so that the central (gut) ray from each fiber strikes the collimator normal to the surface. Thus, the slithead is at the focus of a one-dimensional Schmidt collimator. See §4.1.2 for more details on the slithead design.

The spacing of the fibers on the slit was determined from an analysis of the flux contamination due to crosstalk at the detector between adjacent spectra. In our design we leave gaps between each fiber spectrum to accommodate the shuffled spectrum. Assuming an object four magnitudes fainter than the sky (e.g. a galaxy and sky with magnitudes 24 and 20, respectively), and using error functions to model the profile of the spectra in the spatial direction, we calculated the signal contamination from the adjacent sky spectra as a percentage of the galaxy flux. With a 14 pixel fiber-to-fiber spacing at the detector (the spectra are 5 pixels tall), and using SDSS camera PSFs, there is less than 1% contamination of the *galaxy's light* from the two adjacent nod & shuffled sky spectra. The WFMOS camera design discussed below has tighter PSFs than the SDSS cameras, so we feel very comfortable with this spacing. At the slithead, this results in 292 fibers on a 560 μm center-to-center spacing yielding a total slit length of 163.5 mm.

3.1.2. Collimator

In combination with the curved slithead, the spherical collimator mirror forms a corrector-less Schmidt collimator. The mirror itself is fabricated from a rectangular Hextek borosilicate blank, 175 mm wide, 483 mm tall, and 73 mm thick. The planar blank is slumped by Hextek's gas-fusion process to near-net radius and then ground and polished to the final radius of 1264 mm. The collimator is the largest optic in the spectrograph and drives the overall height of the optical bench. The longer slit for WFMOS requires the collimator to be ~ 64 mm taller than in the SDSS design.

The collimator forms a pupil at the center of curvature of the mirror, and this is where the gratings are located in each channel in order to minimize their required size.

3.1.3. Beamsplitter

A dichroic beamsplitter divides the incident collimated beam, reflecting the blue portion of the bandpass ($\lambda < 640$ nm) and transmitting red wavelengths ($\lambda > 640$ nm). Note this has been tweaked from SDSS's 600 nm dichroic split, due to the extended bandpass out to 1 μm. It is fabricated from fused silica, 229 x 271 x 38 mm, with the dichroic coating applied to the incident surface. Based on the SDSS beamsplitters, the coating will reflect the blue light very efficiently ($R > 99\%$) and transmit the red light somewhat less efficiently ($T > 92\%$ average, including the reflection loss at the exit surface, which has a high performance broadband antireflection coating). The 10%–90% zone at the crossover wavelength is approximately 50 nm wide.

3.1.4. Gratings

Like the SDSS spectrographs, a grism immediately follows the beamsplitter in each channel. However, the significant increase in efficiency offered by VPH gratings[7] convinced us to abandon the SDSS replicated grism design in favor of a VPH grism. The grism consists of a VPH transmission grating sandwiched between two right prisms; the use of two right prisms preserves the straight-through beam layout of the SDSS design.

The WFMOS preliminary design calls for a ruling density of 612 l/mm in the red channel and 842 l/mm in the blue channel; apex angels are 26.8° and 23.3°, respectively. The grisms were designed independently at JHU (using the ZEMAX raytrace program) and at Kaiser Optical Systems, Inc. (KOSI), who also provided preliminary efficiency curves based on rigorous coupled wave analysis (RCWA). Recent measurements at JHU of the new VPH grisms for LDSS-2, which are similar to the WFMOS design, showed ~ 90% peak efficiencies and support our enthusiasm for using these gratings in WFMOS.

For WFMOS, we believe VPH gratings will increase the throughput by more than 45% over that realized by the SDSS spectrographs (see §3.2.3).

3.1.5. Cameras

The cameras are very similar to those used in the SDSS spectrographs, which were designed by Harland Epps. The all-refractive approach was taken to maximize throughput, because placing the detector or a secondary mirror in the unobstructed beam produced by the fibers and collimator would result in significant light loss. The SDSS cameras employ eight lens elements arranged in five groups, including a contact triplet, a contact doublet, and three singlets. All the surfaces are spherical except for the air side surface of the second element in the doublet, which is a relatively mild asphere. Careful attention was paid to glass selection in order to maximize throughput at 390 nm, with five of the eight elements being either calcium fluoride (CaF_2) or Ohara i-line glasses (which have > 98% internal transmission at 365 nm). Dow Corning Q2-3067 optical coupling gel was used to join the elements in the doublet and triplet.

The WFMOS cameras present a more challenging design than SDSS, due to the significantly larger field of view (20.6° vs. 16.5°) and the extended wavelength coverage. A preliminary design has been identified, using the same glasses and element configuration as the SDSS cameras, but with a second aspheric surface. The 240 mm focal length is preserved, the overall length of the camera is increased by 15 mm, and the diameter of the larger lenses has grown by about 6% (the longer slit produces significantly higher beam angles from the collimator). The second asphere is located on the rear surface of the first element, which is made of CaF_2 and could be diamond-turned and post-polished for a modest premium over a spherical surface.

3.1.6. Detectors

For the WFMOS low resolution spectrograph, we have assumed $4k^2$ CCDs with 15 μm pixels. This represents a 25% increase in the physical extent of the CCDs over SDSS ($2k^2$ with 24 μm pixels), and allows us to maintain ~ 300 fibers per spectrograph with nod & shuffle while preserving the basic design, layout, and resolution of the SDSS spectrographs. The 200 μm fibers are imaged to 75 μm by the cameras, which corresponds to 5 pixels on a 15 μm pixel CCD.

The choice of particular CCD devices is most important from an instrument efficiency standpoint, and is discussed in §3.2.3. A commercial CCD, the e2v CCD44-82, is currently available and is a good match for the instrument. This device is a 2k x 4k array in a 3-side buttable package. However, the recent acquisition of a larger "stepper" (the lithographic equipment used to step-and-repeat the mask layout on the silicon die) now makes it possible for e2v to produce a $4k^2$ version of this device. The single monolithic array is simpler to mount and align, will not leave a gap in the middle of the spectrum, and is less expensive than two 2k x 4k devices. For these reasons we have selected the $4k^2$ format.

With the standard astronomy broadband AR coating, the CCD44-82 QE is excellent over the blue channel bandpass. For the red channel, deep depletion CCDs offer much improved response at 1 μm. The CCD44-82 is available in a deep depletion version with an NIR coating, as would be the $4k^2$ version of the device, and would be quite a good match for the red channel. Even better would be the fully depleted devices developed at Lawrence Berkeley National Laboratory,

which have significantly better response beyond 8000 Å than the e2v devices. Throughput curves assuming each of these devices are presented in §3.2.3.

3.2. Optical Performance

The following sections will describe the optical performance of the WFMOS low resolution spectrograph, including image quality, spectral resolution, and instrumental throughput. Comparisons with the SDSS spectrograph performance will be discussed as well.

3.2.1. Image Quality

Spot diagrams for the red and blue channels are shown in Figure 2 and Figure 3, respectively. The spots are shown within a 75 µm diameter circle, representing the imaged fiber diameter on the detector. Each diagram covers the full respective bandpass of the channel, and field points covering the full length of the slit. In general the WFMOS camera design produces smaller spots than the SDSS design (spot diagrams not shown here), which leaves some performance headroom available for fabrication and alignment tolerances, or perhaps for other cost reduction (e.g., matching of vendor test plates).

3.2.2. Spectral Resolution

To analyze the spectral resolution, defined as $\lambda/\Delta\lambda$, where $\Delta\lambda$ is taken to be the spectral FWHM of the slit image on the detector, the following procedure was used. In ZEMAX, a circular source the diameter of the fiber was placed at the slit location having the largest RMS spot size for the wavelength under consideration. Many thousands of rays were launched from this circular source with a uniform distribution, and the resulting image recorded on a simulated detector with pixels ¼ the size of the assumed 15 µm CCD pixels, in order to better sample the image. The simulated image data was exported and analyzed to determine the FWHM, *without* collapsing the image. The FWHM thus determined was taken to be $\Delta\lambda$, and the results are plotted in Figure 4. For a given wavelength, the spectral FWHM and resolution of the WFMOS design are similar to the SDSS spectrographs.

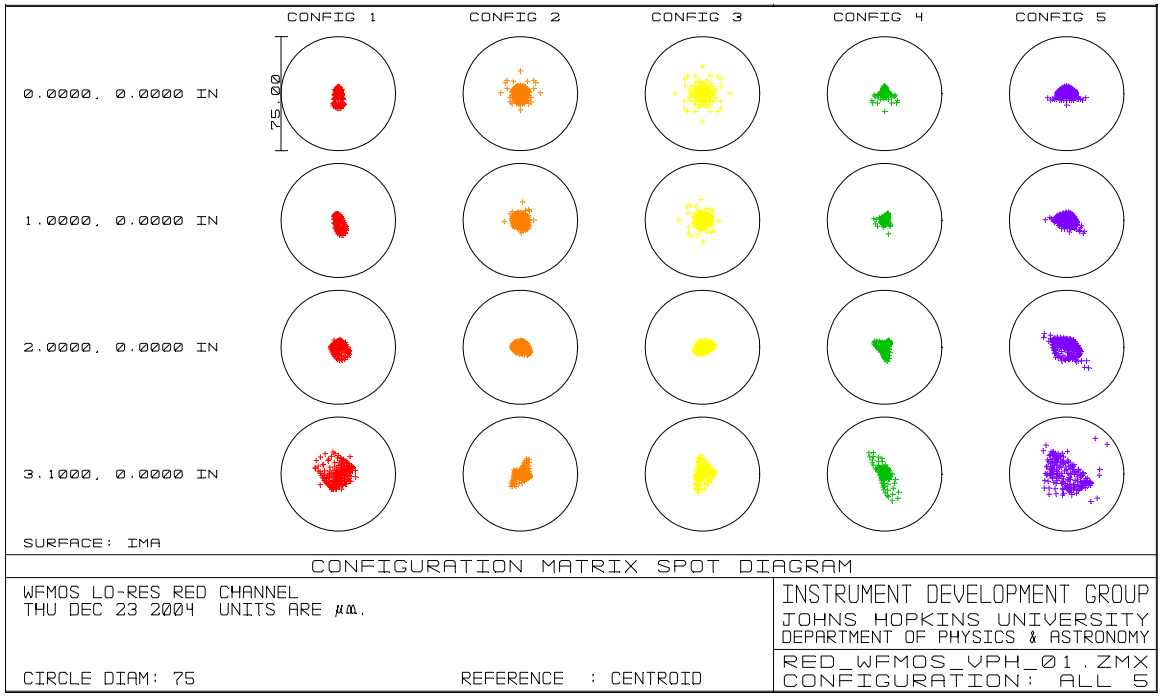

Figure 2. Spot diagrams for the red channel. The circles are 75 µm in diameter, corresponding to the size of the fiber image on the detector. Rows represent a particular position along the slit, from center (top row) to end (bottom row), indicated by labels to the left of each row. Each column represents a particular wavelength. From left to right they are: 1000, 900, 806, 710, 625 nm.

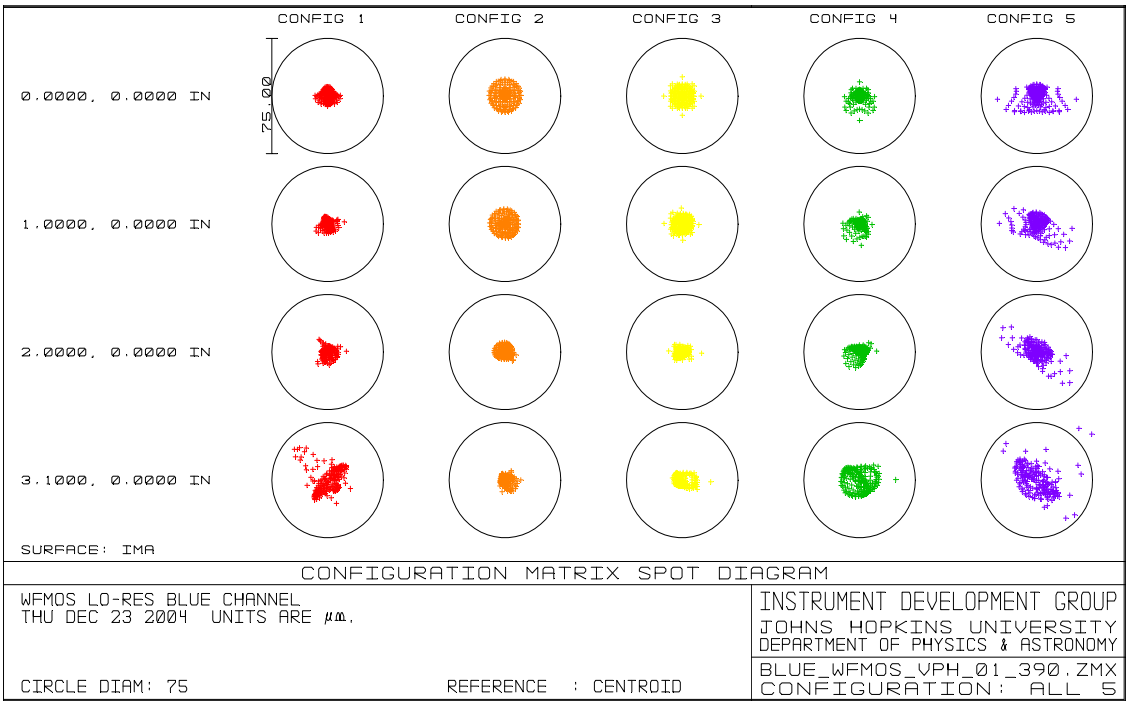

Figure 3 Spot diagrams for the blue channel. From left to right the wavelengths are: 655, 586, 516, 460, 390 nm.

In reality, the resolution of the instrument will be determined using collapsed spectra, so the resolution as reported here is on the low side. However, the ZEMAX analysis assumes perfect optics and alignment, so it is prudent to be conservative at this stage. It is worth noting that the SDSS cameras were reported to perform exactly as predicted by raytrace using the as-built prescriptions.

Higher resolution than the SDSS design is beneficial in the red channel for OH line suppression. By pushing the dichroic cutoff to ~ 690 nm and increasing the speed of the cameras to f/1.4 and f/1.2 in the blue and red channels, respectively, we can increase the resolution in the red channel to ~ 3 Å (R = 3300 at λ = 1 μm) while maintaining the SDSS resolution in the blue channel. These changes would come at a modest cost compared to the overall instrument budget. Pushing the resolution higher than this would involve a reduction in simultaneous wavelength coverage and the addition of rotating grism mounts, or major changes to the design to maintain full simultaneous coverage of the bandpass.

3.2.3. Throughput

The SDSS spectrographs form the basis for the efficiency model developed for the WFMOS low resolution spectrographs. The model for SDSS consists of component efficiencies as a function of wavelength for the following: atmospheric extinction, telescope, fibers, collimator, dichroic, grism, camera, and CCD. *Measured curves* were used for the collimator, dichroic, grism, camera coatings, and CCD QE. Internal transmission curves for the camera glasses were obtained from the manufacturer's data sheets. The telescope and fiber efficiencies came from the SDSS spectrograph purple book.[8] Figure 5 shows measured end-to-end throughput curves for the both of the SDSS spectrographs. The curves are taken from the JHU SDSS web site[9] and the model curve is derived from the component efficiency model described above. The agreement between the model and measured curves is very good.

Having thus validated the component efficiency model with real measurements from the actual instrument, we can apply the same model with confidence to predict the efficiency of the WFMOS low resolution spectrographs based on the similar SDSS instrument design. Figure 6 shows the modeled efficiencies for everything prior to the spectrographs. The 4-layer protected silver coating was used for the Gemini primary, while for Subaru an aluminum coating was assumed.

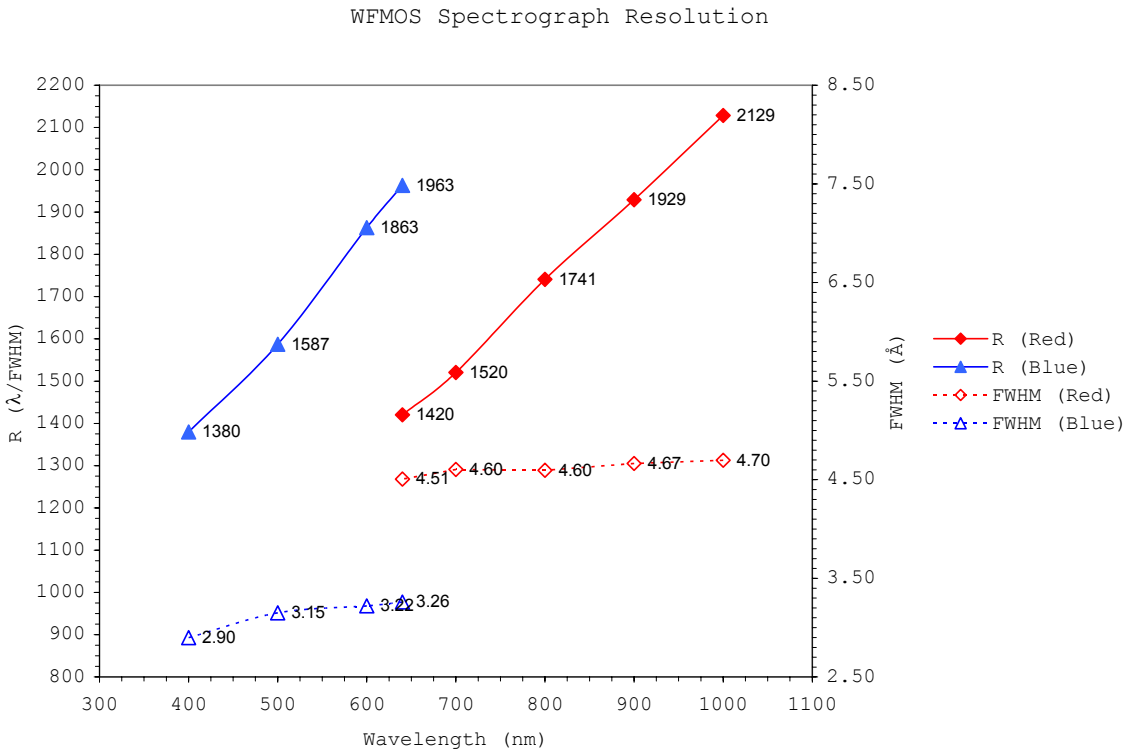

Figure 4. Resolution and spectral FWHM for the WFMOS spectrograph design.

Fiber lengths of 60 m and 40 m were assumed for Gemini and Subaru, respectively. Due to the aluminum coating and shorter fiber run, Subaru is more efficient below ~ 460 nm.

Figure 7 shows the spectrograph component efficiencies for both channels. Two curves are shown for VPH grisms for each channel. One is the RCWA prediction from KOSI for a preliminary, unoptimized grating design, which has been derated by a hefty 10% from the theoretical curve. The other is from recent measurements of the new LDSS-2 VPH grisms performed at JHU. The LDSS-2 grisms are similar in design to the WFMOS grisms, and were manufactured by Wasatch Photonics (WP) and bonded to prisms at JHU. We have chosen to use the measured LDSS-2 efficiencies for the throughput predictions presented here.

Figure 8 shows the instrumental efficiency prediction for the WFMOS low resolution spectrographs. Curves are shown using the VPH grisms as well as exact replicas of the SDSS grisms. Note that we have not done any optimization of the grating designs or efficiency curves to try to compensate for the dip in overall efficiency near the dichroic split. Clearly the use of VPH grisms will enhance the efficiency of these spectrographs significantly over that realized by SDSS, so much so that VPH gratings are the baseline and we are no longer considering the use of conventionally ruled and replicated surface-relief grisms. KOSI and WP (formerly Ralcon) gratings are now used in spectrographs at many observatories.

Another enhancement to the SDSS spectrograph efficiency comes from improved CCD response. The SITe CCDs used for SDSS had excellent QE but employed a broadband AR coating that peaked just longward of 600 nm and fell rather rapidly beyond 700 nm. With AR coatings better matched to the two bandpasses and enhanced red sensitivity offered by high-resistivity deep depletion devices, significant gains in efficiency will be realized in both channels, but especially in the red, for WFMOS. Figure 7 shows curves employing two possible CCDs for the red channel: e2v's deep depletion NIR device and Lawrence Berkeley Lab's high-resistivity, fully depleted device, which has significantly better response longward of 800 nm. For the blue channel, an e2v device with the astronomy BBAR coating was assumed for all four WFMOS curves shown.

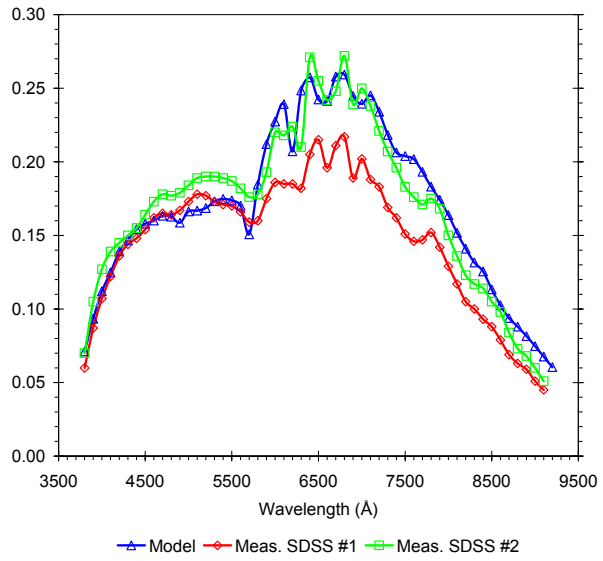

Figure 5. Component model throughput prediction and measured end-to-end throughput for the as-built SDSS spectrographs.

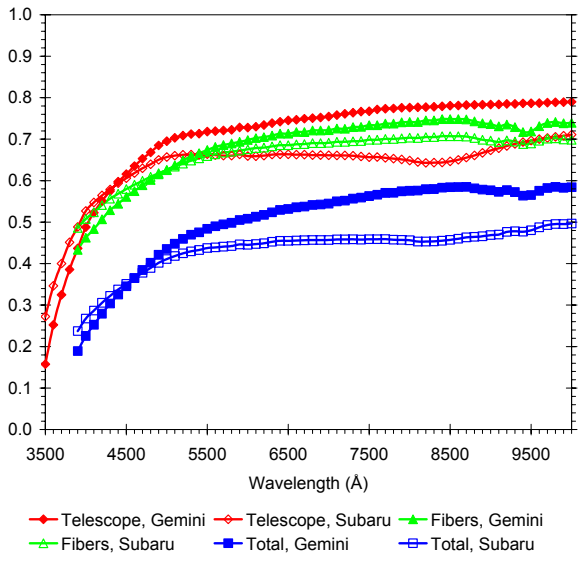

Figure 6. Front-end (non-spectrograph) efficiencies used in the WFMOS model for both the Gemini and Subaru telescopes. The telescope curves include the atmosphere, primary, and corrector; fiber curves include transmission (both 100 and 200 µm fiber runs), air/glass interfaces, fiber connector, and vignetting loss.

The combination of VPH gratings and better CCDs provides an increase in peak instrumental efficiency from 45% for SDSS to 74% for WFMOS (using LBL CCDs for the red channel; the peak is 70% using the e2v CCDs). *This factor of 1.6 improvement in throughput comes entirely from two demonstrated technologies and thus we feel our numbers are extremely robust.*

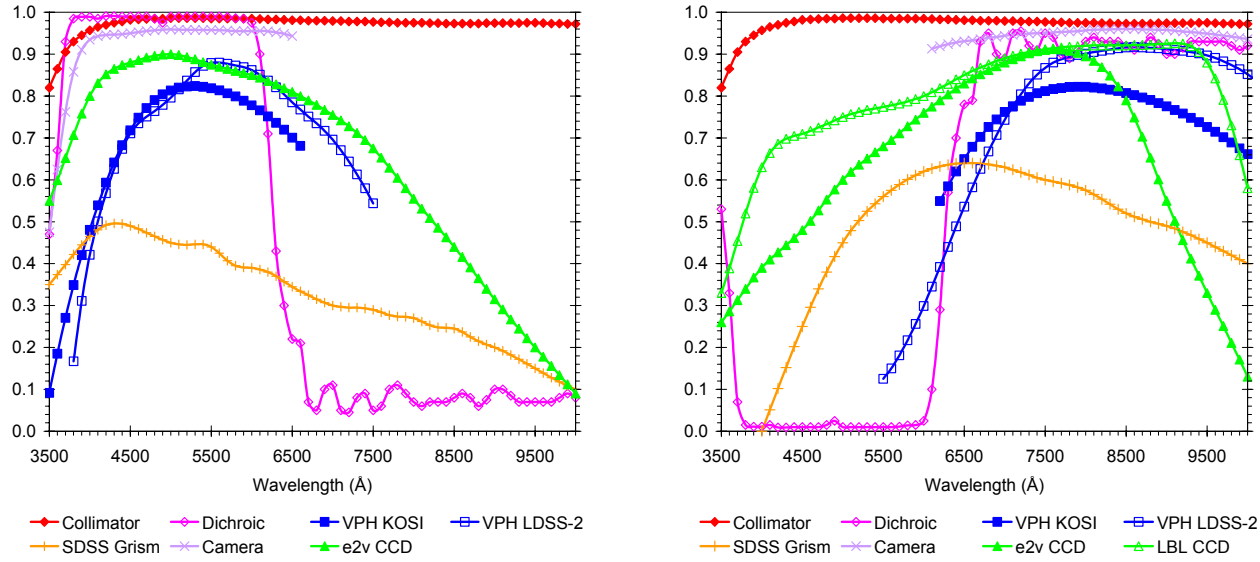

Figure 7. WFMOS spectrograph component efficiencies used in the model model: (left) blue channel and (right) red channel.

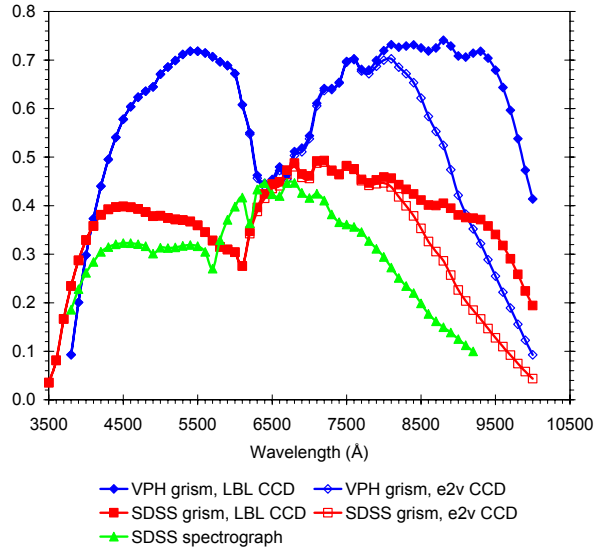

Figure 8. Instrumental efficiency predictions for the WFMOS low resolution spectrographs. The SDSS spectrograph curve, extracted from the model, is shown for comparison.

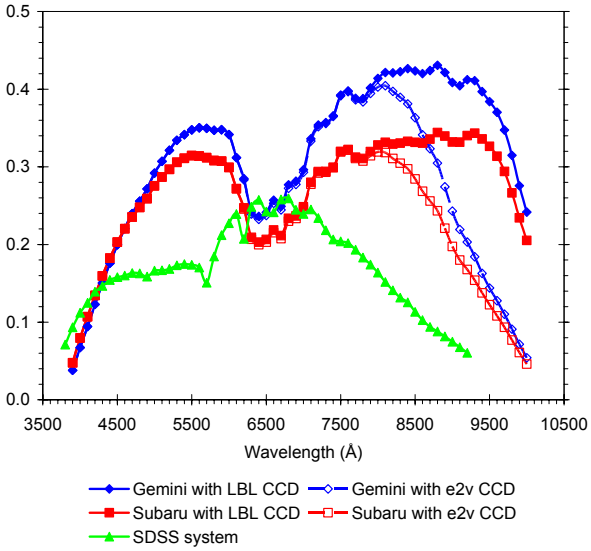

Figure 9. End-to-end throughput predictions for the WFMOS low resolution spectrographs. Note that aperture/seeing losses are not included here.

Figure 9 shows the predicted end-to-end throughput from the model on both Gemini and Subaru, with the SDSS curve included for comparison. The peak throughput of the WFMOS spectrographs on Gemini with LBL CCDs is 43%, more than a factor of 1.6 increase over SDSS at 26%. On Subaru, with an aluminium coating on the primary and less efficient fiber coupling, the peak throughput is 34%, still a factor of 1.3 higher than SDSS. And Subaru is slightly better than Gemini below 460 nm. This throughput performance compares with the baseline KAOS Purple Book peak of 23% for single channel low-resolution gratings, and represents almost a doubling of the integrated photon flux between 400 and 1000 nm. Table 1 gives the integrated flux relative to the Purple Book prediction for both telescopes and choice of red channel CCD.

We re-emphasize that while these results are spectacular they are based on well-tested component efficiencies, and to the best of our knowledge exceed the performance of any fiber spectrograph built to date.

Table 1. Relative integrated photon flux from 400–1000 nm.

Purple Book Fig. 3.1.29	Gemini LBL CCDs	Gemini e2v CCDs	Subaru LBL CCDs	Subaru e2v CCDs
1.00	1.92	1.63	1.64	1.40

4. MECHANICAL DESIGN

4.1. Overview

The mechanical design, like the optical, follows closely from that of the SDSS spectrographs, which have performed very reliably over the past seven years. For SDSS, the twin spectrographs were mounted on the telescope. This was done to minimize the repeated bending of the fibers that would occur with floor-mounted spectrographs, as well as minimizing the length of the fibers. With telescope-mounted spectrographs, flexure in the optical bench was critical, and it was also important to protect the optics from dust and condensation. The mechanical design thus incorporates a

closed, stiff optical bench. While not as strictly necessary for the WFMOS spectrographs, this proven heritage does have the advantages of protecting the optics environmentally, as well as protecting the optics mechanically and maintaining alignment during handling. Hence, given the proven on-sky performance, reliability, and design heritage of the SDSS spectrographs, we have chosen to maintain the overall mechanical design and simply scale it to meet the WFMOS requirements.

Figure 10 shows a rendering of the WFMOS low resolution spectrograph. It is for the most part a scaled version of the SDSS design. If compared side-by-side one would notice only a subtle difference in dimensions. For WFMOS the height is increased to accommodate the taller collimator. The width is also increased slightly to make room for larger grisms and slightly larger cameras. The increased size of the optics is dictated by the desire to take full advantage of a larger detector, thus maximizing the number of fibers per spectrograph. The overall length, width, and height of the instrument are ~ 2230 mm x 1000 mm x 570 mm, respectively. The instrument mass is 318 kg. Like the SDSS design, all optical subassemblies (i.e. the slit assembly, collimator, central optics, and cameras) interface to a common, enclosed optical bench. Each of these subassemblies is described in more detail below.

4.1.1. Optical Bench

A principal design goal during the development of the SDSS spectrographs was to simplify alignment of optical components mounted to the optical bench. To achieve this goal, it was decided that, wherever possible, adjustments would be eliminated in favor of precision machined interfaces that would guarantee accurate and repeatable component placement. This objective, combined with the flexure and environmental requirements, led to the enclosed optical bench shown in Figure 10. Though the flexure and environmental requirements for WFMOS are far less stringent, the nicety of being able to assemble the instrument without time-consuming adjustments, as well as design heritage and robustness, make the SDSS bench design a logical choice for WFMOS.

Figure 11 shows the optical bench and the optomechanical subassemblies that interface to it. The dual-channel optical design naturally leads to the *T*-shaped layout depicted in the figure. In this configuration, the red and blue channel cameras, as well as the collimator assembly, mount to exterior faces of the bench; one at the end of each leg of the *T*. The fiber slithead and the central optics assembly, which contains the dichroic and grisms, are mounted internally. At all of these subassembly interfaces precision machined reference datums exist to facilitate accurate placement, hence

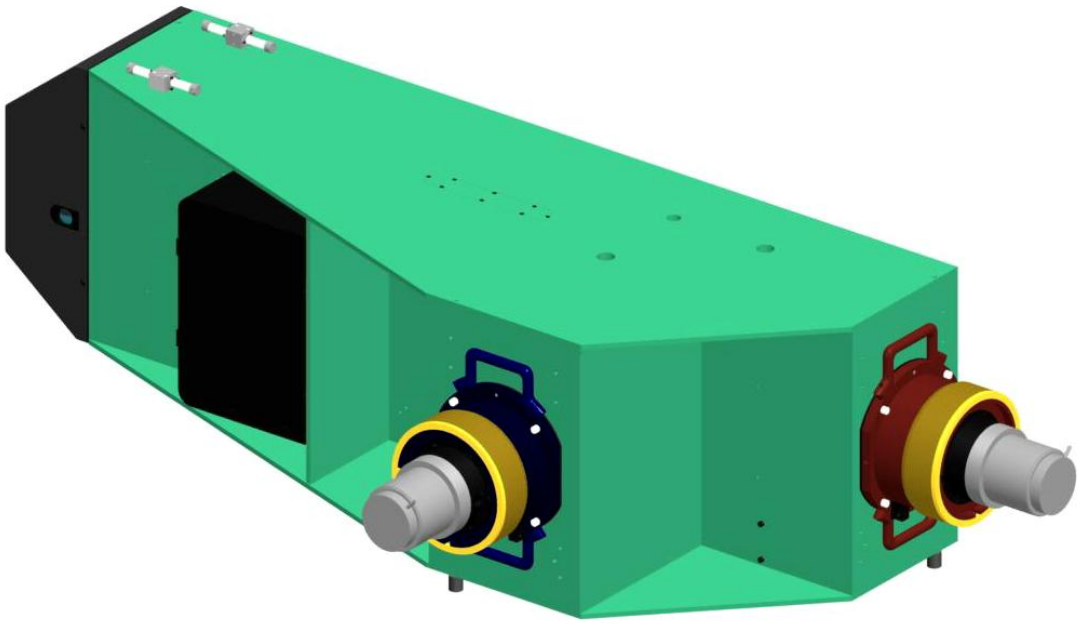

Figure 10. Rendering of the WFMOS low resolution spectrographs.

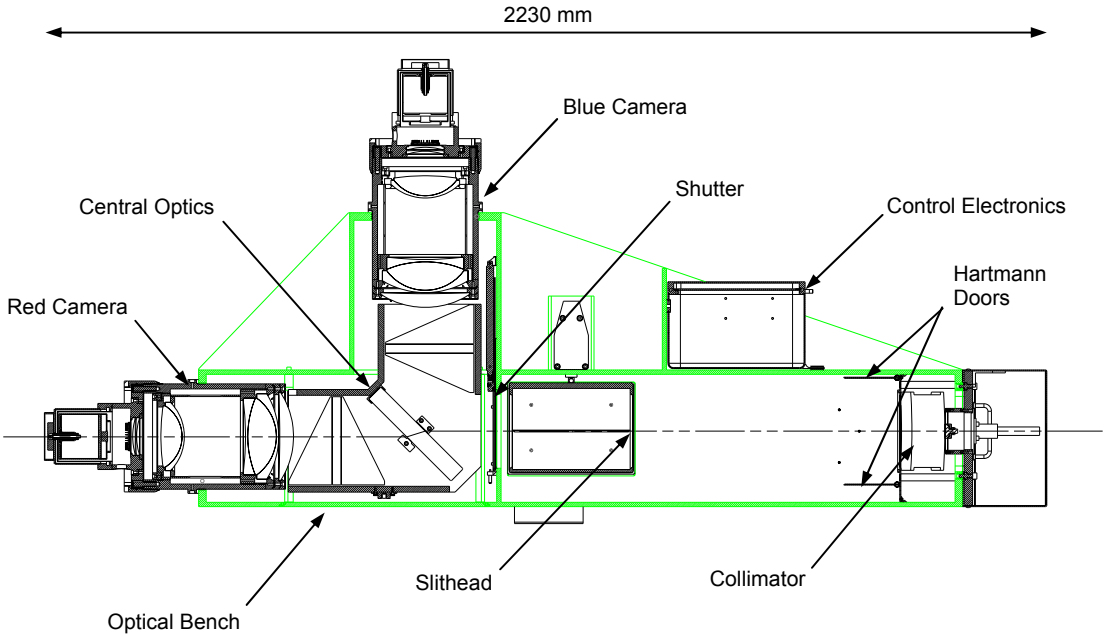

Figure 11. WFMOS low resolution spectrograph optomehcanical layout. Optomechanical subassemblies interface to the optical bench at machined interfaces dramatically reducing the number and complexity of adjustments. The central optics subassembly contains the dichroic and the grisms.

guaranteeing alignment. Instrument control electronics and CCD controllers (not shown) mount to exterior walls of the bench.

4.1.2. Slithead

Fibers enter the spectrograph through the slithead, which serves as the optomechanical interface between the fibers and the optical bench; see Figure 12. As shown in the figure, the slithead is a box-like structure, with openings in the front and rear faces so that light reflected by the collimator can pass through the system. Fiber bundles (20 fibers per bundle) enter through the bottom, gently bend along the surface of a thin vertical plate, the slit plate, and then terminate along an arc concentric to the collimator; each fiber being normal to the collimator. The array of terminated fibers constitutes the spectrograph entrance slit. The slit plate spans the vertical extent of the slithead and vignettes a small portion of the beam. It provides strain relief for the fibers and the curved leading edge serves as a gage for mounting the fibers on the correct arc.

The slithead mounts kinematically to the side wall of the optical bench. Two tooling balls at the top of the structure engage a conical socket and a v-groove affixed to the optical bench. A third tooling ball, mounted to the base of the optical bench side wall, contacts a hardened surface on the side of the slithead. The slithead is held in place by a single pneumatic clamp that seats all three interfaces. The kinematic mount guarantees repeatable placement; a requirement for the SDSS spectrographs since slitheads are exchanged for each field observed. While not strictly necessary for WFMOS, this kinematic mount is robust, economical, and desirable should the unit have to be removed to repair a damaged fiber.

4.1.2.1. Fiber Back Illumination

Like the SDSS spectrographs, a fiber back-illumination system is required to map the location of fibers in the focal plane to their respective positions on the slit. WFMOS has the same requirement but the implementation is somewhat different. Here the fiber back-illumination system must be an integral part of the spectrograph since the slithead will not be removed from the spectrograph between observations. For Sloan, the plug plate and its companion slitheads are integrated into a single assembly, the fiber cartridge, which is configured off-line prior to observing. This off-line

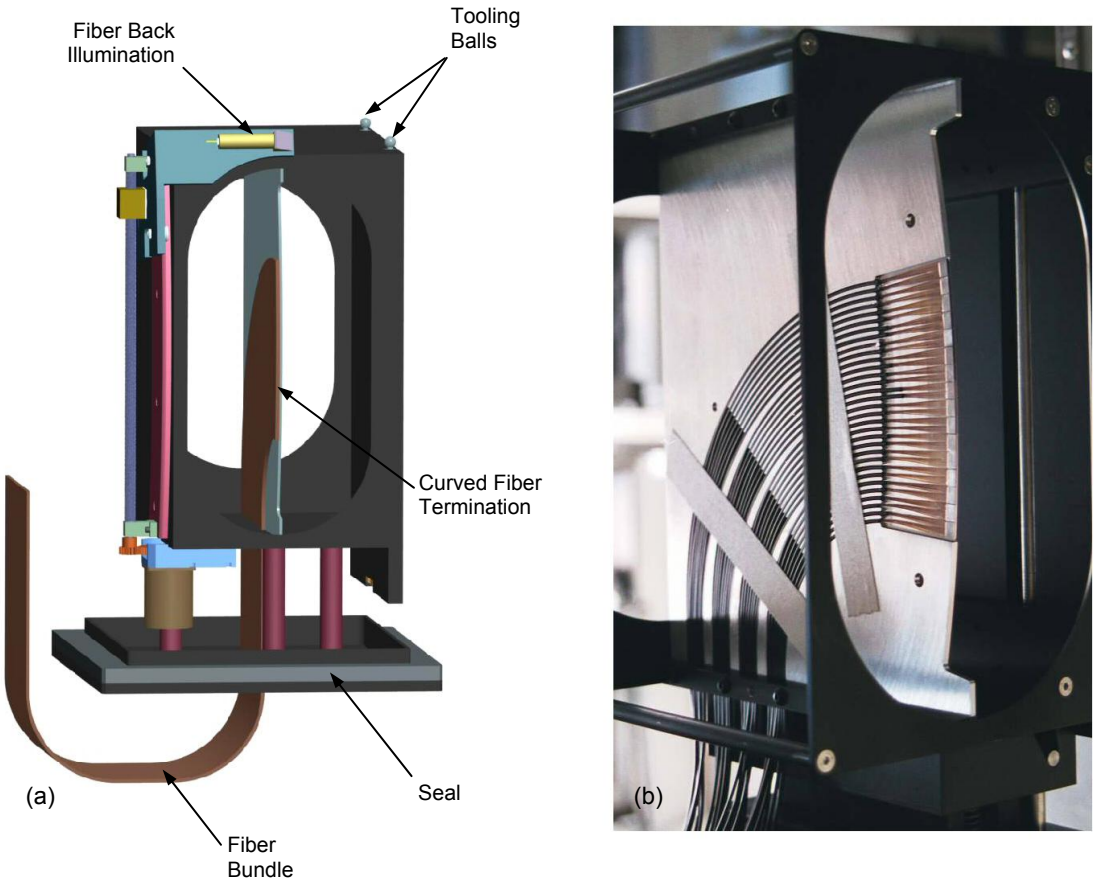

Figure 12. (a) Slithead design. The fibers terminate along the curved edge of the central vertical plate; the radius of curvature being half the radius of the collimator. A fiber back-illumination system scans the slit illuminating fibers in the focal plane. (b) Image of the SDSS slithead showing fiber routing, fiber strain relief and termination.

configuration made it possible to have a single back-illumination system that would temporarily mount to the slithead, map the fibers, and then be removed prior to wheeling the cartridge to the telescope for installation and observing.

The fiber back-illumination system for WFMOS is similar to the SDSS system, however it is an integral part of the slithead; see Figure 12. Fibers are illuminated sequentially in scanning mode by a source focused on the front of the slit. As the head scans along the slit the fibers are illuminated one by one. A remote camera will image the focal plane and centroids will be determined.

The back-illumination system is a relatively simple mechanism. The source module consists of an LED, a fold mirror, and a lens to reimage the LED source on the fiber. The module is mounted to the carriage of a curved translation stage that is driven by a stepper motor and lead screw. When parked, the head resides at the top of the slithead clear of the beam. The system is designed to scan the 292 fiber slit in 15 seconds (an additional 15 seconds is required to return the head to the park position), which is negligible compared to the overall observation overhead. As specified, the system could scan the head much faster, or slower, by simply adjusting the motor speed.

4.1.3. Collimator

The collimator mount provides remote tip/tilt and focus adjustment. An initial focus adjustment can compensate for surface radius variation from nominal, allowing for less critical fabrication tolerances on the mirror and optomechanics. More frequent adjustments can compensate for seasonal temperature variations. A pair of Hartmann doors is located in

front of the mirror to allow shifts in the collimator focus to be measured rapidly. Tip/tilt adjustment allows the collimator to be precisely coaligned to the cameras, or at least to an average of the two camera axes. Thus, the center fiber can be positioned at the center of the detector in the spatial direction, and the central wavelength can be positioned at the center of the detector in the spectral direction.

Details of the motion control system are depicted in Figure 13. The mechanical configuration is fairly simple. The mirror is supported from the back surface, at its center, by a circular membrane flexure (not visible in the figure). This flexure constrains the mirror in-plane but allows out-of-plane compliance for tip, tilt, and piston adjustment. The out-of-plane control is provided by three linear actuators that also attach to the back of the mirror. Motion of each actuator is limited (by limit switches) to ± 3 mm. The linear actuators as well as the fixed edge of the membrane flexure are attached to a common mounting plate, which is the interface to the optical bench. A shim between the mounting plate and the optical bench facilitates one-time, gross focus adjustment. Accurate and repeatable assembly of the subsystem is made possible by two dowel pins (one round and one diamond shape) that engage hardened bushings pressed into the optical bench (this scheme is also used to locate the cameras). Safe installation is facilitated by two handles for lifting and four guide rods that flank the collimator and ensure the collimator clears the bench opening as it is installed. A cover protects the actuators and helps cut down on stray light.

The linear actuators used for the SDSS spectrographs were DC-Mike actuators from Physik Instrumente. These devices consist of a micro DC servomotor, gearhead, lead screw, and encoder packaged in a round slender form-factor. They provide submicron resolution (~ 0.3 μm), which is more than sufficient for this application; the required resolution is ~ 1 μm.

4.1.4. Hartmann Doors

A pair of bi-fold Hartmann doors reside just in front of the collimator stop and are used to perform a Hartmann test,

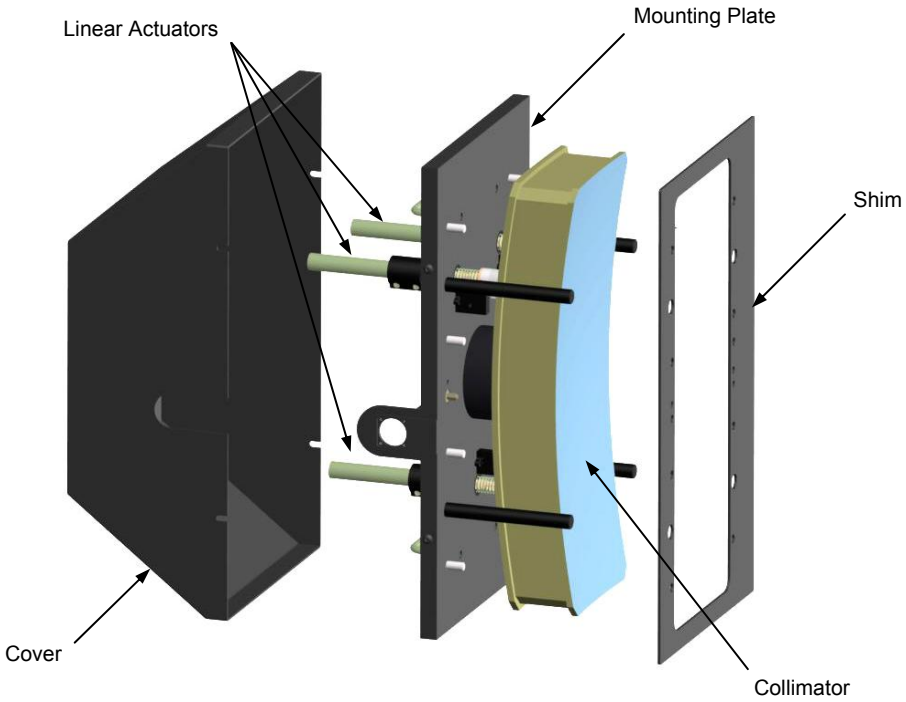

Figure 13. Collimator mount and position control. The collimator is supported in-plane by a membrane flexure and out-of-plane by three linear actuators. The three actuators provide tip, tilt, and piston control of the collimator. A shim between the mounting plate and the optical bench facilitates course, one-time, focus adjustments.

which enables quick determination of focus. Any out-of-focus condition is corrected by a piston adjustment of the collimator. Since the red and blue channels of the spectrograph are parfocal the piston adjustment focuses both channels simultaneously. Note that the parfocal condition is achieved by a manual adjustment of the cameras, which occurs seasonally.

The doors are driven by simple, 90 degree, pneumatic rotary actuators. Actuation of these devices is controlled by the embedded controller in the spectrograph electronics box.

4.1.5. Shutter

A single shutter is used to control the exposure in both channels. It is located just upstream of the dichroic on a dividing wall in the optical bench; see Figure 11. With the shutter at this location the beam is blocked to both channels when closed.

The shutter is a simple sliding-door mechanism consisting of a pneumatic cylinder, a door, and door frame. The single piece frame has slots to guide the door and a large window sized to match the beam profile; hence the door frame doubles as a light baffle. Aside from guiding the door, the slots also produce a light tight seal when the door is closed. The spectrograph microprocessor controls the cylinder which opens and closes the door.

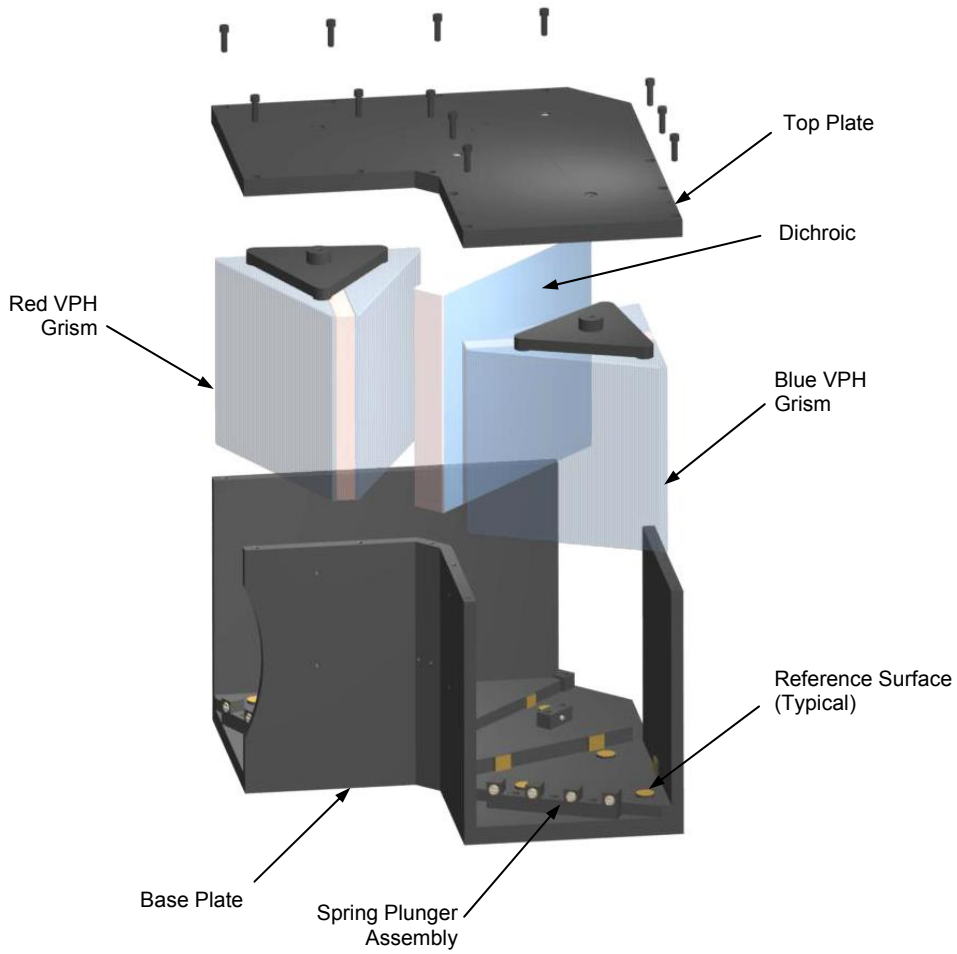

Figure 14. Optomechanical details of the central optics assembly. The dichroic and both grisms are each kinematically located by six reference surfaces. Spring plungers constrain the elements to these surfaces and accommodate differential contraction between the glass and the aluminum structure.

4.1.6. Central Optics

The dichroic and VPH grisms are located in a single optomechanical structure, the *central optics* assembly, located just behind the shutter. The assembly is kinematically mounted inside the optical bench on three machined posts; two of which have concentric sleeves that engage the assembly and orient it in-the-plane. The *L*-shaped structure is 15% larger and 40% more massive than the SDSS assembly due to the taller slit (which necessitates a taller dichroic and grisms) and the use of VPH grisms.

Figure 14 shows the details of the central optics assembly. The dichroic and both grisms are each located, without adjustment, by six machined reference surfaces. Spring plungers seat the elements against the reference surfaces and accommodate differential contraction between the glass optics and aluminum structure. To minimize tolerance stack-up and improve placement accuracy, all but one of the eighteen reference surfaces is machined into a single component, the *base plate*, the bottom side of which interfaces to the optical bench. The remaining reference surface is located on the top plate and it controls the tip of the dichroic. Placement accuracy of this last surface hinges on tolerance stack-up within the structure, which was not an issue for the SDSS version of this design.

4.1.7. Camera Optomechanics

The SDSS camera design (shown in Figure 15) serves as the baseline for the WFMOS low resolution spectrograph cameras. Like its predecessors (the Keck Low-Resolution Imaging Spectrometer, and the Norris spectrograph at Palomar) the lenses and lens-groups are mounted in athermal cells. The cells are bolted together in series and mounted in a common barrel. Reference diameters machined concentric to the lens bores establish lens concentricity from cell-to-cell. This technique has been successful in the past for the lens sizes, materials, and configuration described above (see §3.1.5) making it a logical approach for WFMOS.

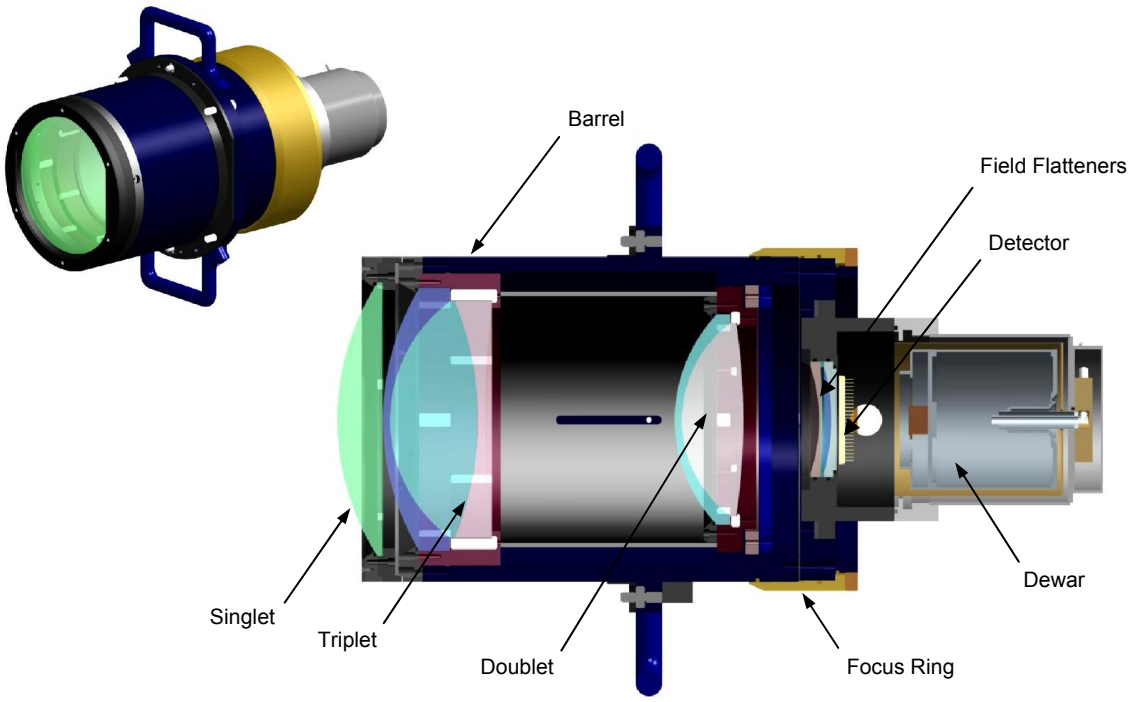

Figure 15. Optomenchanical design of the SDSS cameras (blue camera shown here). Lens elements are mounted in cells which are mounted in a common barrel. The focus ring translates the dewar assembly, which contains the field flatteners. This focus adjustment is used strictly to make the two channels parfocal.

The design and construction of the athermal cell design is best described as follows. A metal ring with an appropriate coefficient of thermal expansion is bored oversize to the as built lens diameter. Six glass-filled Teflon plugs are lightly pressed into a hole pattern circumscribing the lens bore. These plugs are then bored on a lathe to a diameter that just clears the as-built lens diameter. In the same machining step, the lens axial locating faces and cell reference diameters are machined, thus achieving lens concentricity (within the limits of radial clearance) and perpendicularity to the optical axis. The plug diameter is calculated such that the net change in the diameter of the finished bore is less than the diametrical clearance to the lens over the temperature range of interest, given the coefficients of expansion for the metal ring, the Teflon plug, and the glass lens. Where lens groups are packaged in a single cell, multiple sets of plugs are used. For the SDSS cameras, aluminum was used for the singlet and doublet cells, and steel was used for the triplet cell. A Kapton shim is used between the lens locating face and the cell. An o-ring between the retaining ring and first lens surface provides force to seat the lens and compliance to accommodate differential expansion. A rendered image of the triplet cell depicting these details is shown in Figure 16.

In the SDSS camera, the singlet cell attaches to the front of the triplet cell, which in turn attaches to the front of the outer camera barrel. The doublet cell is metered with respect to the triplet by a steel inner barrel. The length of this barrel and the thickness of a shim between the singlet and triplet cells are optimized for the as-built lens dimensions. Contact and compliance between the doublet cell and inner barrel is achieved using an array of stiff springs that push against the back face of the doublet cell.

The field flatteners are mounted in the front dewar flange just in front of the detector. The entire dewar is manually translated for focus adjustment using the focus ring on the OD of the camera barrel. This adjustment is used strictly to

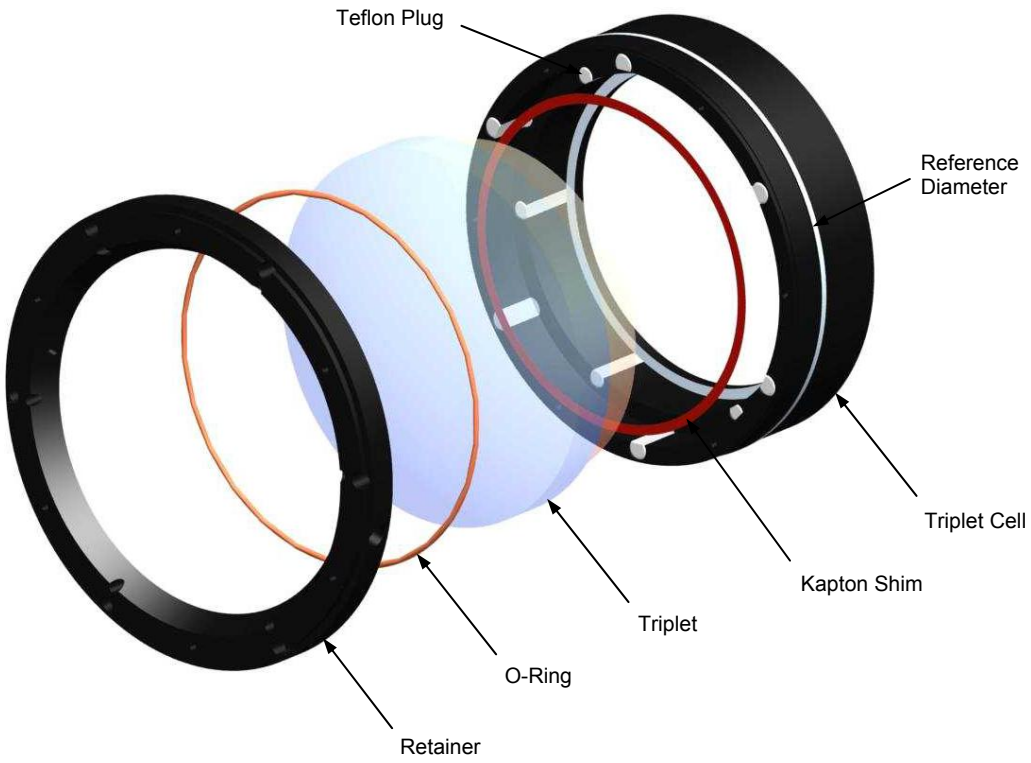

Figure 16. SDSS triplet cell. Glass-filled Teflon plugs are bored to fit the as-built lens diameters. Reference surfaces machined in the same setup guarantee accurate placement of the elements within the barrel. An o-ring between the retainer and first surface of the triplet retains the lenses and accommodates differential expansion between the glass lenses and metal cell.

make the two channels of the spectrograph parfocal. Routine focus compensation is done using the automated piston adjustment of the collimator.

For WFMOS the detector will most likely be cooled by a closed cycle refrigeration system as opposed to LN_2, which was used for SDSS. Modifying the back end of the camera to accept this change should be straightforward. The detector mount however should be nearly identical, in concept, to the SDSS design. We envision that the $4k^2$ array package would be nearly identical to the SITe detectors used for Sloan; hence, the invar mount and the three point adjustment scheme would suffice for WFMOS. The mount will have to be scaled, of course, to accommodate the 25% increase in detector size.

5. ACKNOWLEDGMENTS

This work is based upon work supported through AURA Contract No. 0084699-GEM00385, and by funding from the Johns Hopkins University.

6. REFERENCES

[1] C. Blake, K. Glazebrook, "Probing Dark Energy Using Baryonic Oscillations in the Galaxy Power Spectrum as a Cosmological Ruler," *The Astrophysical Journal*, 594, 665-673 (2003)
[2] http://www.noao.edu/kaos/KAOS_Final.pdf
[3] K. Glazebrook, J. Bland-Hawthorn, "Microslit Nod-Shuffle Spectroscopy: A Technique for Achieving Very High Densities of Spectra," *The Publications of the Astronomical Society of the Pacific*, 113, 197-214 (2001)
[4] I. J. Lewis, et al., "The Anglo-Australian Observatory 2dF facility," *Monthly Notices of the Royal Astronomical Society,* 333, 279-299 (2002)
[5] P. Gillingham, S. Miziarski, M. Akiyama, and V. Klocke, "Echidna – a Multi-Fiber Positioner for the Subaru Prime Focus," *Proceedings of the SPIE*, 4008, 1395-1403 (2000)
[6] D. G. York, et al., "The Sloan Digital Sky Survey: Technical Summary," *The Astronomical Journal*, 120, 1579-1587 (2000)
[7] S. C. Barden, J. A. Arns, and W. S. Colburn, "Volume-phase holographic gratings and their application for astronomical applications," *Proceedings of the SPIE*, 3355, 866-876 (1998)
[8] www.astro.princeton.edu/PBOOK/spectro/spectro.htm
[9] http://www.jhu.edu/~sdss/Spectrographs/Throughput.html